Multiple regression based prediction correlations for enhanced sensor design of magnetic induction tomography systems

Arellano, Y., Hunt, A., Haas, O., Ahmed, H. & Ma, L.

Multiple regression based prediction correlations for enhanced sensor design of magnetic induction tomography systems

Yessica Arellano[1], Andrew Hunt[2], Olivier Haas[3], Hafiz Ahmed[3] and Lu Ma[2*]

[1] Fluids and Complex Systems Research Centre, Coventry University, Coventry, UK
[2] iPhase Limited, Unit 7 Intec Business Park, Basingstoke, UK
[3] Research Institute For Future Transport and Cities, Coventry University, Coventry, UK

E-mail: luma@iphaseflow.com[2]

Abstract

Magnetic Induction Tomography (MIT) is an imaging technology that measures changes in the electric properties of a sample located within the imaging region. Measurement of low conductivity contrasts such as biological tissue or ionized water flow in pipelines requires highly accurate systems due to the small amplitude of the measured signals. Optimisation of the sensors results in enhanced MIT performance. Geometric characteristics of MIT sensors impact the intensity of the electromagnetic field, and the inductive coupling between a) the sensors and b) the sensors and the medium. Three correlation models are derived to help developers predict the relative performance of MIT systems for a given set of coil characteristics. Bivariate and multiple regression analyses are performed on a dataset from Finite Element Method (FEM) simulations to validate the relationship between the sensor geometry and three performance parameters for a given set of uniform background distributions. Correlation models are provided for prediction of induced voltage level, eddy currents and system sensitivity relative to the geometric characteristics of the sensors. The performance of the computed models is validated using a dataset of 180 coil designs and four uniform electrical conductivity distributions. Predictions from the developed correlations are compared to reference data from simulations and experiments. Errors estimated for the predicted performance parameters together with the variance for each correlation are presented. The predicted data fitted the reference values within ±15%, showing reasonable accuracy of the models and a balanced variance-bias trade-off. It was found that the performance of MIT systems is largely affected by the coil dimensions and the number of turns, as well as by the coil shape and wire diameter to a lesser degree.

Keywords: Magnetic Induction Tomography, sensor design, multiple regression

1. Introduction

Magnetic Induction Tomography (MIT) is an imaging technique for measurement of electrical properties through

electromagnetic induction [1]. MIT systems for low conductivity measurement comprise an array of sensors that are typically positioned around the circular perimeter of the container [2], [3], [4] The sensors measure changes in the electromagnetic field distribution due to the induction of eddy currents in a conductive medium. The received signal encompasses information from the primary induced magnetic field and the secondary eddy current field. The secondary field provides information inherent to electromagnetic properties of the species within the imaging region. Hence, the distribution of the electric properties of conductive inclusions can be inferred from changes in the measured signals.

MIT is attractive for biological tissue imaging, and ionic water transport monitoring due to its ability to detect low conductivity contrasts on differently hydrated layers and in multiphase pipelines [5], [6]. Low conductivity imaging requires high excitation frequency and high-resolution equipment. At high frequencies, the skin depths of the electromagnetic fields are comparable to the target dimensions and the signal arising from the induced eddy currents is only a fraction of that of the primary magnetic field. The amplitude measurements from low conductive medium imaging is a few orders of magnitude smaller than the driving input resulting in weak and noisy signals [7].

Several MIT systems have been designed over the past three decades, most of which rely on circular helix coils sensors [2], [8], [9], [10], [11], [12], [13], [14]. The reason for this selection is, however, not well elaborated in the literature. The performance of MIT systems largely depends on the intensity of the induced field and currents. The inductive coupling between the sensors and the medium is influenced by the hardware design, including the sensors [15]. Limited literature has addressed the sensor optimisation design for MIT, suggesting the use of alternative geometries [16] and manufacturing techniques [17].

This paper is an extended version of the work published in [18], where a systematic evaluation of the effect of sensor design on selected performance parameters was performed. Expectedly, from [18], large numbers of turns and small wire cross sections provide enhanced sensitivity and large coil couplings. Furthermore, square helix coils induce larger voltages and increase the system sensitivity in contrast to circular geometries. The degree of association of the coil geometric parameters to the system performance variables is, however, still unknown.

MIT signals are proportional to the electrical and physical properties of the inclusions which, depending on the process, can vary in both spatial and time domain. The nature of the problem presents significant challenges in defining models for non-continuous conductivity distributions which are representative for the target of interest and that address a range sufficiently wide to encompass all possible scenarios.

Consequently, the present study focuses on the design parameters of MIT sensors for a uniformly distributed conductive medium. This approach allows quantifying the performance of the MIT system in connection to the overall variations of the electrical properties within the medium and to the design of the system.

This paper assesses combined variations of the sensor geometry. The design parameters comprise the traditional circular-shaped coils as well as square helixes. The sensor size, wire gauge and number of turns are also addressed in this study. The dimensions of the coils and the size of the saline inclusion used in this work consider the theoretical spatial resolution and skin effect in low conductive fluids. This study also combines variables whose influence on the MIT performance is not straightforward, namely the wire gauge and the number of turns. The number of turns is known to affect the mutual coupling and the parasitic capacitance [13], [19]. However, the impact of the number of turns, combined with other geometry parameters, on the induced voltage resulting from the secondary magnetic field arising from flow-induced eddy current is yet to be quantified. Moreover, at high frequencies, the current density across the wire cross section is not uniform, due to the skin effect of the copper.

Statistical procedures provide quantitative tools to assess the relative importance of the geometric variables on the MIT performance. All the procedures used in this work are based on inferential statistics, which allow the testing of specific hypotheses about the sensor geometry [20]. The two main types of inferential tests have been adopted in this work: the tests of association to describe the relationship between variables and the tests of group differences for data dispersion analysis and correlation validation.

A comprehensive evaluation of the impact on the MIT performance of the changes in the coil design parameters was performed. The results presented in this work are based on both numerical simulations and experimental tests of a dual coil MIT system. Numerical results are analysed here through a combination of statistical techniques that comprise bivariate correlations, uniqueness indices, and multiple regressions. The bivariate association tests can provide a measure of the statistical significance, a measure of association between variables, or both [20]. Spearman test provides a measurement of both significance and association. Furthermore, Spearman correlation coefficient measures the degree of correlation between a pair of combined variables i.e. ordinal and continuous, irrespective of their linearity or lack thereof [20],[21]. Aimed at non-parametric data, the Mann-Whitney test is an alternative bivariate test for variable association irrespective of the data distribution shape [22]. The ideal unique variance accounted for in the bivariate performance factors is valid as long as two ideal conditions hold: (a) the independent and dependent variables show strong

correlations, and (b) the independent variables demonstrate weak correlation with each other. Computation of the relative importance of geometric parameters on the overall system performance is achieved through multiple regression analyses. Multiple regression provides the model that best fits the behaviour of the data. Similarly to the correlation approach taken for data processing from experiments in multiphase flow [23], curve fitting coefficients are used to describe the performance of the MIT systems via correlation models.

This paper extends the simulation studies performed in [18] and move from a descriptive analysis to an inferential exploration in order to develop, for the first time, algebraic models to help researchers predict the overall performance of MIT systems for a given coil setup. In the following sections, the influence of sensors geometry (i.e. size, wire gauge, number of turns and profile) on the intensity of the induced signals and system sensitivity for uniform conductivity distributions is studied.

The outcome is exploited in the optimisation design process and factor correlations are provided to describe MIT performance for a given sensor geometry. The correlations presented here are the best fits to describe the behaviour of the data. These correlations have the potential to help researchers predict the relative overall performance of MIT systems for given coil setups. The proposed models allow enhanced sensor designs without the need to perform experimental tests or simulation work.

2. Methodology

The methodology adopted in this work comprises the following stages:
- Perform numerical simulations with varying coil geometries to assess changes in the receiving signals.
- Perform experimental tests on selected coil geometries.
- Analyse the induced fields and the amplitude of the signal from the evaluated sensors using statistics.
- Derive correlations that describe the performance of MIT systems with respect to the sensor design.
- Validate the derived correlations by contrasting the predicted value to reference data.

The following subsections describe the model setup, the computational approach used to solve the electromagnetic problem numerically, and the data processing techniques.

2.1 System Setup

The MIT experimental setup is based on the dual coil system, illustrated in Figure 1. The dual coil assembly greatly simplifies the numerical model and the analysis process.
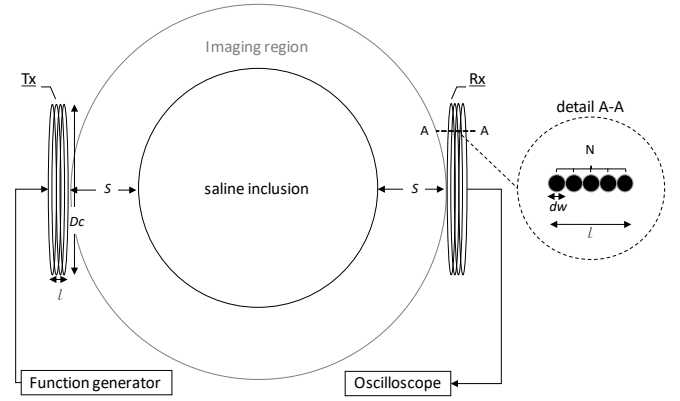
Figure 1. System setup for sensor geometry characterisation showing the profile of generic transmitting and receiving coils of outer dimensions Dc, N turns and wire diameter dw.

The system used for evaluation accounts for a pair of coils, each of which acts as transmitting (Tx) and receiving (Rx) sensors. The system illustrated in Figure 1 shows the system setup with generic coils of outer dimension Dc formed with N turns of wires of diameter dw.

In the experimental setup the coils were located across a circular imaging region of 110 mm in diameter. The transmitting coil was voltage driven via a function generator (GW Instek AFG-2125) at 5 V_{pp} with an operating frequency of 10 MHz. The excitation signal induces a magnetic field that is sensed by Rx, located at 180º from Tx. Rx is connected to a digital oscilloscope (PicoScope 5444B) that measures the induced voltage and phase in the receiving sensor for further data processing. A cylindrical saline inclusion of 70 mm in diameter was used to evaluate the sensitivity of the MIT system to changes in conductivity. The inclusion was placed in the centre of the imaging region equidistantly from Tx and Rx.

2.2 Numerical simulations

A broad range of geometry parameters were evaluated using CST Student Edition®. The solution of the numerical model involves solving the governing equations of the electromagnetic phenomena for the entire domain. For a time-harmonic field with linear materials the problem is described by Maxwell's equations in (1)

$$\nabla \times \mathbf{E} = -j\omega\mathbf{B}$$
$$\nabla \times \mathbf{H} = \mathbf{J} + j\omega\mathbf{D} = (\sigma + j\omega\varepsilon)\mathbf{E} + \mathbf{J_s}$$
$$\nabla \cdot \varepsilon\mathbf{E} = \rho \qquad (1)$$
$$\nabla \cdot \mu\mathbf{H} = 0$$

where **E** and **H** are the magnetic and electric fields, **B** and **D** are the magnetic and displacements currents, respectively, and **J** is the current density. The electrical properties are given by the permeability (μ), the conductivity (σ), and the permittivity

(ε). ω is the angular frequency, ρ is the electric charge density, and $\mathbf{J_s}$ is the source current density.

The boundary value problem governed by (1) is solved via volume discretisation with Finite Element Method (FEM). FEM discretises the integral form of Maxwell's equations for all subdomains. The distribution of the unknown parameters within each domain is interpolated from the values of the edges (edge FEM). The external boundary condition forced a zero normal component of the field. Placing the external boundary conditions far away from the electromagnetic source, allow a sensible approximation to the decay of the field [7]. The simulation model exploits the CST Student Edition® software capability to improve mesh quality in the area of interest by using the numerical approximations of stranded inductors enclosed in dummy objects. The coil domain ensures a closed current path in agreement with Maxwell's equations. This condition is satisfied by introducing an excitation source across an infinitesimal cross-sectional slit. The coil domain function assumes the source is outside the modelling domain and in doing so it provides the possibility to model alternative features outside the coil array. The sensing coils were modelled as open circuits with the electromotive force computed from (2) representing the maximum potential difference when no external load is connected.

$$V_{Rx} = \oint \mathbf{E} \cdot dl \qquad (2)$$

where V_{Rx} is the induced voltage in the receiving coil and dl is the length element of the coil.

The induced voltage, induced current density, electric and magnetic field distributions were computed for 180 scenarios. Two data sets, each accounting for 90 coil configurations, were simulated. The first dataset (see Table 1) was used to find the correlation between the sensor geometry and the MIT performance parameters. Dataset 2 was used to validate the correlations derived using Dataset 1 and assess the ability of the correlations to extrapolate as well as to interpolate among the given range. The simulation campaign accounted for a systematic variation of the geometry of the sensors that resulted in a total of 180 coil configurations. The simulation combination comprised three coil outer dimensions (Dc), three wire diameters (dw), five numbers of turns (N) and two coil profiles, i.e. circular and square helixes, for each dataset. Furthermore, the system performance for various conductive mediums was assessed changing the electrical conductivity (σ) of the homogeneous saline inclusions.
The simulation model was validated against experimental results of selected sensor geometries and readily known responses for changes in electric properties of the conductive medium placed between the sensors.

Table 1. Geometric parameters for geometry correlation and for validation

	Dc (mm)	dw (mm)	N	σ (Sm^{-1})	*Profile*
Dataset 1	25	0.50	2	0	CH[a]
	34	0.60	6	1	SH[b]
	50	0.75	10	5	
			14		
			18		
Dataset 2	20	0.40	4	0	CH[a]
	40	0.55	8	1	SH[b]
	54	0.85	12	3	
			16	5	
			20		

[a]Circular helix coils.
[b]Square helix coils.

2.3 Statistical analysis

The degree of association among the geometric variables and selected MIT performance parameters was assessed through bivariate correlations. For ordinal data, i.e. Dc, dw, and N, the Spearman correlation factor was used to measure association between variables and their statistical significance. The relative correlation between the variables and the nominal predictors (i.e. coil profile) was assessed using Mann-Whitney tests.

The quantification of the change of the mean levels of the variables was analysed through a comparison of multiple regressions. Through the Analysis of Variance (ANOVA), the overall regression correlations were tested to ensure a good fit for the dataset. The correlations that presented the best fit for every performance parameter, based on tests of group differences, were selected and further validated. The validation of the correlations accounted for contrasting the predicted values to reference figures from the two datasets and the experimental results. The resulting equations expressed the MIT performance including the sensitivity, denoted S_i; the ratio of the amplitude measured by the receiving sensor (V_{Rx}) to that of the transmitting sensor (V_{Tx}), denoted V_i; and the magnitude of the induced conduction current J_i in terms of the coil outer dimensions (Dc), the wire diameters (dw), the number of turns (N) and the coil profiles G.

2.4 Optimisation of the problem formulation

The MIT performance indicators V_i , J_i and S_i can be formulated as objectives with Dc , dw , N and G being the design variables. Optimisation algorithms can then be employed to determine the most appropriate values of Dc , dw , N and G to create a suitably optimised MIT sensor design. The software selected to implement the optimisation was MATLAB^{TM}. It is convenient to formulate MATLAB^{TM} optimisation problems as minimisation. The latter requires to

adapt the MIT performance indicators, that should be maximised, by negating them. The performance indicators formulations are designed for the Geometric parameters defined in Table 1. It is therefore required to limit the range of values the design variables can take. The formulation of the optimisation problem for MIT sensor design can be summarised as follows:

$$min \quad f(x), \qquad x \in \mathbb{R}^n$$
$$Subject \ to: \qquad Dc \in [20, 54]$$
$$dw \in [0.40, 0.85]$$
$$N \in [2, 20]$$
$$G \in \{1, 2\}$$

where,

$$f(x) = [-V_i(x), -J_i(x), -S_i(x)]$$

$V_i(x), J_i(x), S_i(x)$ is the objective function evaluated at x

$x = [Dc, dw, N, G]$ is a vector of decision variables.

Two approaches have been adopted to handle the three objectives. The first one was to combine the objectives into a single weighted sum of normalised objectives. The second was to use a Pareto approach where all objectives are considered in parallel. The latter enable to create a set of equally optimal solutions. The solution obtained using the weighted sum is one of the solution found for the specific set of weightings selected by the user. Details on model optimization are outside the scope of this manuscript, however, an example of the problem optimisation is given in section 6.2. Further details can be found in [24].

3. Experimental measurements

In this section, simulation outputs are contrasted to the experimental study carried on selected coils geometry configurations. The analysis aims to validate the extended simulation results to be used for the sensor optimisation. During the experiments, circular and square-shaped geometries were explored. The size of the transmitting and receiving coils was modified in order to account for outer dimensions of 25 mm, 34 mm, and 50 mm.

Measurement of the coil inductance at 5 Khz for various coil profiles and number of turns is plotted in Figure 2. The simulated inductance is contrasted to data measured in the lab and to the measured circuit resonance frequency from coils of 34 mm wound from copper wire of 0.5 mm. The overall trends observed in the experimental measurements coincide with those from simulation. Contrasting the inductance of both square helix (SH) and circular coil (CH), it is evident that consistently larger inductances are measured in square-shaped coils. Furthermore, the data shows a quadratic trend that yields larger differences between both geometries for an increasing number of turns. In this regard, the mean relative change between the square and the circular coils for every
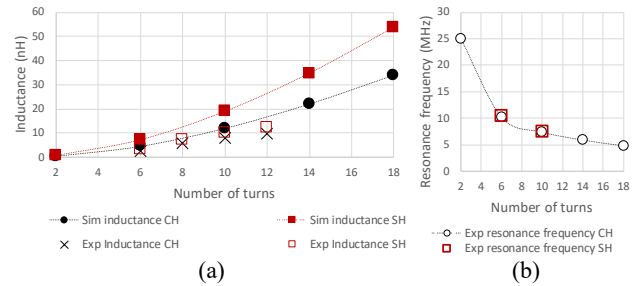

Figure 2. Results for (a) coil inductance and (b) self-resonance frequency of circular (CH) and square helix (SH) for various number of turns

variation in the number of turns are in agreement, with ratios of 0.37 and 0.33 for the simulated data and the experimental points, respectively. The variation evidenced between the measured and simulated inductances is attributed to the frequency of the modelling. As the frequency increases the simulation model is able to capture the change in reactance and the skin effect that are not considered in the low-frequency AC measurements [19].

In accordance with the trend of the coil inductance, the experimental validation of the circuit resonance frequency shows a non-linear tendency (see Figure 2b). Detailed analysis of the self-resonance of the coils with varying wire diameters and dimensions resulted in the number of turns being the governing factor [18]. Accordingly, in the remaining of the paper, the self-resonance frequency is not considered among the performance parameters but it is included as a limiting factor for the maximum number of turns of the coils.

The ratio of induced to excitation voltage for circular and square coils of various number of turns and diameters is presented in Figure 3. The overall simulated and experimental voltage ratio trends are consistent among themselves. However, it is noteworthy that the experimental and simulation results for the circular helix coil of 34 mm and 6 turns differ to the overall trend seen in the remaining data points. This oddity is attributed to the proximity of the operating frequency to the circuit resonance frequency, at which the measured induced voltage peaks. This effect is neglected in the simulations given the numerical approximation used to model the coil domain. Disregarding the outliner above, the absolute mean difference between all the experimental data points and the simulated voltage ratios is 0.06 which corresponds to a mean percent difference of 17%.

4. Performance parameters

Due to the complexity of the eddy current problem, it is challenging to obtain a governing factor that uniquely quantifies the MIT performance. In the present work, various combinations of geometric parameters were tried and judged by their impact on a comprehensive selection of performance
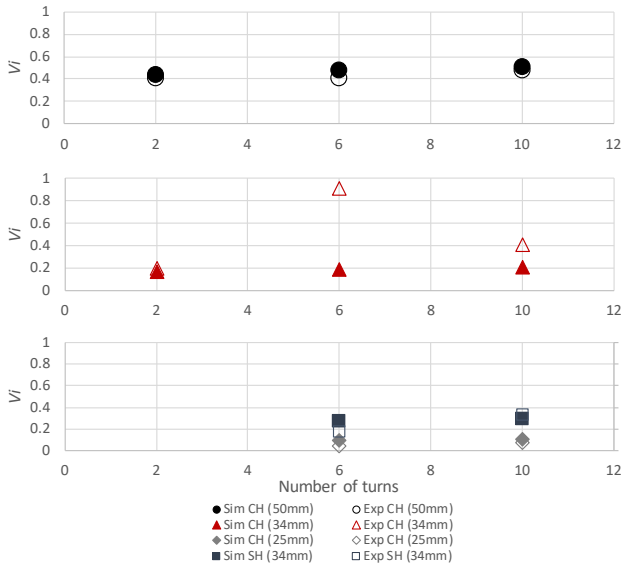
Figure 3. Induced to excitation voltage ratio of circular (CH) and square helix (SH) showing similarities between result from simulations in CST (Sim) and bench tests measurements (Exp) for various diameters and number of turns.

indicators encompassing for the overall system operation. The performance parameters are defined below.

The amplitude of the acquired measurement given by (3) is proportional to the background field generated by the driving signal, hence affecting the signal-to-noise ratio. The performance factor, designated V_i, accounts for the ratio of induced to driving signal as

$$V_i = \frac{V_{Rxi}}{V_{Txi}} \qquad (3)$$

where V_i is the scalar quantity defined by the ratio of the amplitude measured by the receiving sensor (V_{Rx}) to that of the transmitting sensor (V_{Tx}) for scenarios $i = \{1, 2, \cdots, n\}$. In this study the geometry parameters were alternatively changed to account for a total of 90 coil configurations ($n = 90$) corresponding to the Dataset 1 in Table 1.

The signal of interest in MIT systems arises from the induced eddy currents in the conductive medium. The scale of this signal is, however, only a fraction of the full

measurement. An enhanced sensor design should, therefore, account for high induction currents and large rate of penetrations, i.e. skin depths. In this study, the strength of the conduction currents in the imaging region was evaluated along a central longitudinal axis (see Figure 4). The magnitude of the induced conduction current J was computed as the maximum scalar registered within all mesh elements indexed by $\{1, \cdots, m\}$ for every scenario $i = \{1, 2, \cdots, n\}$ ($n = 90$) as in (4). This is given in the equation below

$$J_i = \max_{j \in \{1, 2, \cdots, m\}} (J_j) \qquad (4)$$

where m is the total number of sub-domains along the longitudinal axis.

Equally relevant, is the sensitivity of the system to changes in conductivity within the imaging area. MIT sensitivity is deduced from the Geselowitz relationship expressed as

$$S_i = \frac{\Delta V_{Rxi}}{I_{Txi} \Delta \sigma_i} \qquad (5)$$

where S is the sensitivity of the system for a given change of electrical conductivity ($\Delta \sigma$). I_{Tx} is the current through the transmitting coil. Again, the index $i = \{1, 2, \cdots, n\}$ ($n = 90$) refers to the evaluated scenarios. Note that the original relationship derived by [16] considers the variation of the complex conductivity ($\Delta \kappa = \sigma + j\omega\varepsilon_0\varepsilon_r$). Here, the conductivities evaluated are high ($\omega\varepsilon/\sigma \ll 1$), which allows the application of the eddy-current approximation in accordance to (5) [25].

From (3) to (5) it is inferred that the smaller the values of the performance parameters V_i, J_i, and S_i, the poorer the performance of the MIT system is.

5. Optimisation of the sensor design

The range of the geometric parameters from the dataset 1 is summarised in Table 2. The coil profiles were arranged as circular helix coils (CH) or squared-shaped helixes (SH). The resulting values for each behaviour factor were grouped as per geometry parameter cluster and summed together. The cluster covariance (s_{xy}) serves to identify if any possible
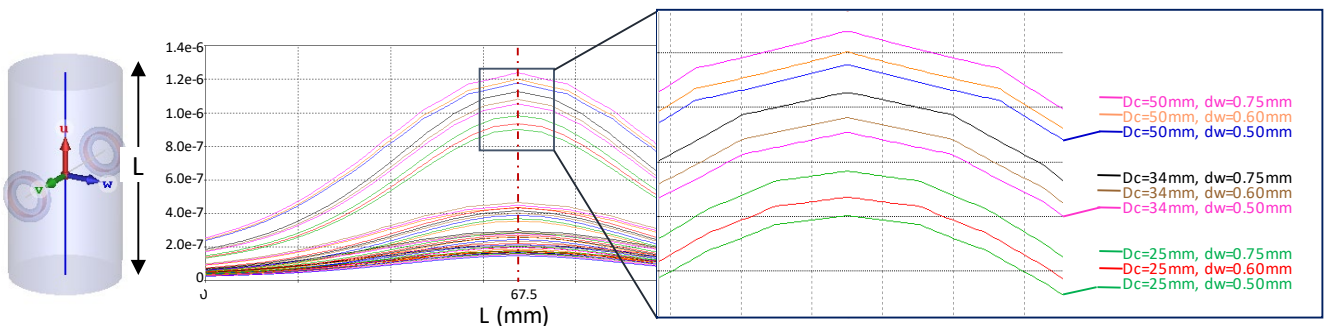
Figure 4 Electromagnetic field intensity [A.m^{-2}] induced by circular helix coils of various diameters, for a given number of turns, measured along the longitudinal axis of the cylindrical imaging region. The vertical grid line signalises the position of the centre of the coils.

Table 2. Result Summary of numerical simulations

Geometric parameter		V_i			J_i			S_i		
		$\sum V_i$	s_{xy}	R^2	$\sum J_i$	s_{xy}	R^2	$\sum S_i$	s_{xy}	R^2
Dc[a]	25	0.017	9.0E-2	9.7E-1	14.99	2.6E-1	7.9E-3	0.01	1.3E-2	4.0E-1
	34	0.033			16.85			0.03		
	50	0.078			18.18			0.10		
dw[a]	0.50	0.042	7.9E-6	7.6E-5	16.34	6.1E-4	4.3E-4	0.05	-1.0E-5	2.6E-3
	0.60	0.042			16.62			0.04		
	0.75	0.043			17.06			0.04		
N	2	0.025	3.8E-5	5.8E-7	26.42	-1.4E+0	7.1E-1	0.00	6.3E-3	3.2E-1
	6	0.026			9.58			0.01		
	10	0.026			6.05			0.02		
	14	0.026			4.45			0.04		
	18	0.025			3.51			0.06		
$Profile$	CH[b]	0.061	2.8E-4	4.0E-3	25.54	-3.5E-3	6.4E-4	0.06	2.9E-5	8.6E-4
	SH[c]	0.066			24.49			0.07		

[a]Measured in mm.
[b]Circular helix coils.
[c]Square helix coils.

relationships among the variables ($s_{xy} \neq 0$) are direct or inverse, i.e., $s_{xy} > 0$ or $s_{xy} < 0$, respectively. The coefficient of determination R^2, given by (6), further validates if the premise of a linear relationship between the variables is correct.

The quantification of the effects of the geometric variables (Dc, dw, N, and profile) on the performance factors V_i, J_i, and S_i and the nature of the predictive relationship was assessed using the statistical procedures detailed in Section 2.3.

$$R^2 = \left(\frac{s_{xy}}{\sqrt{\frac{\sum P_i^2}{n} - \bar{P}^2} \sqrt{\frac{\sum x_i^2}{n} - \bar{x}^2}} \right)^2 \quad (6)$$

where, P_i is the performance parameter, x_i is the geometric factor for scenarios $i = \{1,2,\cdots,n\}$ ($n = 90$) and $\bar{P}$ and $\bar{x}$ are their respective mean values.

From the response of the performance variables to changes in geometric characteristics in Table 2, it is clear that the coil size has the most influence on the induced voltage, with a joint positive variability as by the sign of the covariance and the coefficient of determination. The remaining parameter configurations do not follow a linear relation. However, from the covariance analysis, it is expected for the coil dimensions to also have a large influence on the measurement sensitivity, whereas the number of turns would inversely affect the intensity of the induced currents.

The degree of association among the continuous variables is summarised in the bivariate analysis presented in Table 3 in terms of the Spearman correlation coefficient (ρ) and its significance index (sig<0.05). The authors corroborated that the ideal predictive situation, in which the independent geometric variables display relatively weak correlations among themselves, was met (ρ=0.00, sig=1.00).

Table 3. Analysis of the results using Spearman and the Mann-Whitney correlation methods

		V_i	J_i	S_i
Dc	ρ	0.943	0.147	0.605
	sig	0.000	0.165	0.000
dw	ρ	0.049	0.041	-0.043
	sig	0.647	0.700	0.688
N	ρ	0.009	-0.973	0.748
	sig	0.935	0.000	0.000
$Profile$	sig	0.082	0.218	0.580

Table 4. Multiple regression analysis

	V_i correlation			J_i correlation			S_i correlation		
	Stand. Beta	R²-adjust	Std. error of estimate	Stand. Beta	R²-adjust	Std. error of estimate	Stand. Beta	R²-adjust	Std. error of estimate
Dc	0.991	0.987	0.00134	0.081	0.994	0.02494	0.582	0.998	0.03428
N	0.140			-0.944			0.759		
dw	0.012			0.024			-0.026		
$Profile$	0.066			-0.078			0.058		

The system response for the three performance factors in Table 3 shows mostly positive correlations with the geometric variables. Inverse relations were seen for eddy current induction with increasing number of turns (ρ=-0.973) and for sensitivity for increasing wire gauge (ρ=-0.043). Some geometric parameters were more strongly related to the system performance than others. Accordingly, Spearman coefficient confirmed a strong relationship between the coil size and the induced voltage ratio (ρ=0.943). These outcomes are in agreement with the intensification of sensitivity of the system with increasing sensor size and number of turns. The aforementioned correlations are statistically significant at the 0.05 level.

Conversely, results from the Mann-Whitney tests, applied to the nominal-type data, i.e. coil profile, suggest that the correlation among the performance factors is less statistically significant (sig>0.05) when contrasted between coil profiles; i.e. sig =0.082, 0.218, and 0.580 for V_i, J_i, and S_i, respectively. Through multiple regression analyses, the combined influence of the various geometric parameters on the performance factors was assessed. R^2-*adjusted* in Table 4 displays the quality of the predictions, and allows comparison among the correlations. The developed correlations account for a combination of geometric variables that describe over 98% of the variability of the performance predictors. The *Standardised Beta* coefficients serve to compare the relative importance of the geometric variables. It is evident from Table 4 that the coil diameters and the number of turns were the parameters with the largest impact on the performance factors, followed by the coil profile. The wire gauge was the least relevant one.

The global correlations for every performance factor, given by (7) to (9), were obtained by fitting data with quadratic and

logarithm curves. The ANOVA tests indicate that the ability of the three correlations to predict the performance factors was statistically significant (sig ≤ 0.005). These models provide design guidelines that lead to enhanced sensors design for a wide range of imaging areas and conductivity contrasts.

$$Vi = (a_1Dc + a_3N^2 + a_5N^{0.5} + a_8G + a_9)^2 \quad (7)$$

$$Log(Ji) = a_1Dc + a_2Dc^{0.5} + a_3N^2 + a_4N + a_5N^{0.5} \quad (8)$$
$$+ a_7dw^{0.5} + a_8G + a_9$$

$$Log(Si) = a_1Dc + a_2Dc^{0.5} + a_3N^2 + a_4N + a_5N^{0.5} \quad (9)$$
$$+ a_6dw + a_8G + a_9$$

where the wire diameter, dw, and coil outer dimension, Dc, are expressed in millimetres, σ in S.m⁻¹, F_i are the model parameters listed in Table 5 and G is the profile index, with nominal values of 1 for CH and 2 for SH.

The spread of data around the composite correlations is illustrated in Figure 5. Results showed a significant linear relationship between predicted and reference values with an overall fitting inside the ±15% deviation range. The strong influence of the sensor size is evidenced once more in Figure 5a, where three clear data clusters appear, each corresponding to a given inductor size. Similarly, the dispersion of the data derived from the J_i correlation indicates an inverse relationship between the data and the number of turns irrespective of the conductivity (see Figure 5c and Figure 5d).

Table 5. Correlation constants

|	V_i correlation	J_i correlation	S_i correlation
a_1	0.001119	-0.015762	-0.060902
a_2	-	0.221681	1.246442
a_3	-6.686246E-6	-0.001315	0.002449
a_4	-	0.123560	-0.262666
a_5	0.000934	-0.860193	1.800712
a_6	-	-	-0.186440
a_7	-	0.117432	-
a_8	0.001540	-0.0484915	0.0852280
a_9	-0.009126	$0.1758\sigma - 0.4643$	-11.639089

6. Performance of correlations

The assertiveness in the prediction of the performance parameters was contrasted via the relative performance factor F_{rf}. The relative performance indicator is a modification of the factor recommended by [26] and [27], combining the percent errors described by (10).

$$F_{rf} = \frac{|E_1| - |E_{1\,min}|}{|E_{1\,max}| - |E_{1\,min}|} + \sum_{j=2}^{3} \frac{E_j - E_{j\,min}}{E_{j\,max} - E_{j\,min}} \quad (10)$$

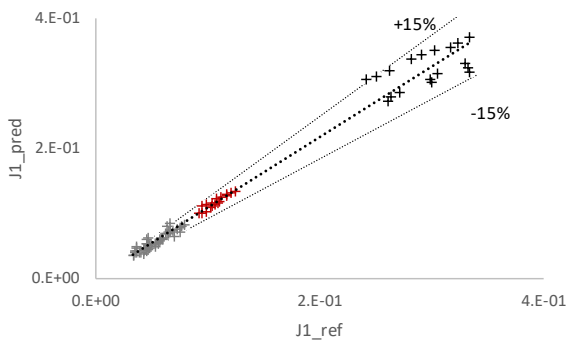where F_{rf} is the relative performance factor and ranges from 0 to 3, 0 being the best relative performance. E refers to the error of the predicted values computed as follows.
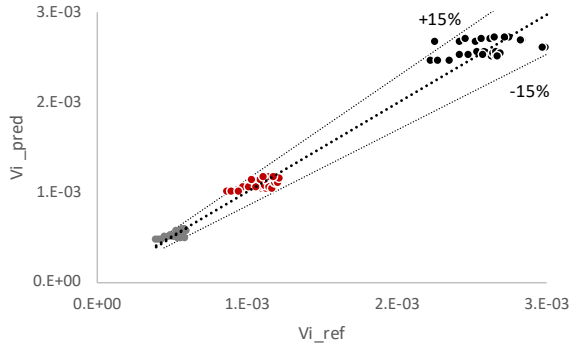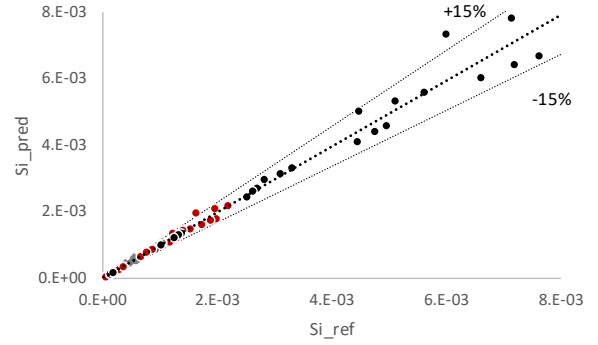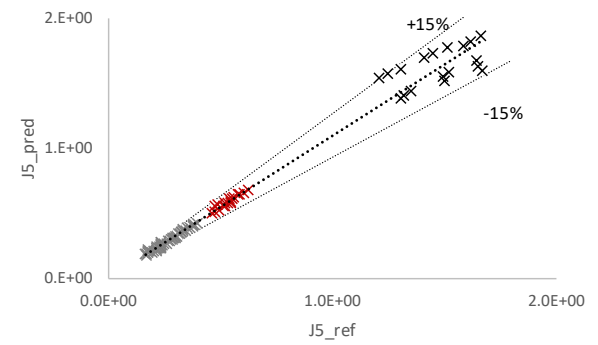

Figure 5. Predicted performance parameters against reference values showing data dispersion around (a) V_i, (b) S_i, (c) J_i for medium conductivity of 1 S.m⁻¹, and (d) J_i for medium conductivity of 5 S.m⁻¹.

$$E_1 = \left[\frac{1}{n} \sum_{i=1}^{n} \frac{(P_i)_{pred} - (P_i)_{ref}}{(P_i)_{ref}} \right] \times 100 \qquad (11)$$

$$E_2 = \left[\frac{1}{n} \sum_{i=1}^{n} \left| \frac{(P_i)_{pred} - (P_i)_{ref}}{(P_i)_{ref}} \right| \right] \times 100 \qquad (12)$$

$$E_3 = \left[\sqrt{\frac{1}{n-1} \sum_{i=1}^{n} \left(\frac{(P_i)_{pred} - (P_i)_{ref}}{(P_i)_{ref}} \right)^2} \right] \times 100 \qquad (13)$$

here P_i are the performance parameters, namely V_i, J_i, or S_i. The suffixes '*pred*'and '*ref*', refer to the predicted and the reference values, respectively. E_1 is the mean percent error and measures the bias in the prediction, indicating the degree of over or under prediction. In the absolute mean percent error (E_2), the signs of the deviations are not considered, which is key in the assessment of the prediction accuracy of the correlations as the positive and negative errors are not cancelled. E_3 is the root mean square percent deviation, which indicates the proximity of the predictions to the reference values.

The absolute deviations were also computed via the statistical parameters E_4, E_5, and E_6, given by (14)-(16). These errors are similar to E_1, E_2, and E_3 but are expressed in absolute magnitude terms non-relative to the reference values.

$$E_4 = \frac{1}{n} \sum_{i=1}^{n} (P_i)_{pred} - (P_i)_{ref} \qquad (14)$$

$$E_5 = \frac{1}{n} \sum_{i=1}^{n} \left| (P_i)_{pred} - (P_i)_{ref} \right| \qquad (15)$$

$$E_6 = \sqrt{\frac{1}{n-1} \sum_{i=1}^{n} \left((P_i)_{pred} - (P_i)_{ref} \right)^2} \qquad (16)$$

E_4 is the mean error and predicts the agreement between predicted and reference measures relative to the reference parameter. E_5 and E_6 are the mean absolute and the root-mean-square errors, respectively.

The variance (s^2) of the difference between the reference and predicted variables is derived for every correlation from (17).

$$s^2 = \left\{ \frac{1}{n} \sum_{i=1}^{n} \left[\frac{(P_i)_{pred} - (P_i)_{ref}}{(P_i)_{ref}} \right. \right.$$
$$\left. \left. - \left(\frac{1}{n} \sum_{i=1}^{n} \frac{(P_i)_{pred} - (P_i)_{ref}}{(P_i)_{ref}} \right) \right]^2 \right\} \qquad (17)$$
$$\times 100$$

Note that the second term on the right hand side of the equation is the mean of the data points for every scenario $i = \{1,2,\cdots,n\}$ ($n = 90$).

6.1 Overall Evaluation

The global evaluation considered all four geometric parameters and three prediction correlations in order to study their combined performance. The evaluation was first performed using the numerical results from the Dataset 1. Subsequently, to validate the models, and make the evaluation unbiased a second database, Dataset 2 in Table 1, was used for geometric parameters inside and outside the initial evaluated range.

Table 6 shows the accuracy of the predictions of all three correlations using both datasets. The evaluation using Dataset 1 led to the errors listed in Columns 2 to 5 of Table 6. The deviations computed using Dataset 2 are shown in Columns 6 to 10 of Table 6.

The outputs from the correlations show consistency based on the computed statistical variances, s^2, which were lower than 4% for all models and datasets. The relative performance factor was systematically larger when the correlations are validated outside the range from which they derived, i.e. for Dataset 2. The V_i correlation provided the most precise predictions as by the relative performance indicator, followed by the S_i model. Predictions of eddy currents (J_i) resulted in the largest deviations with an absolute mean percentage error of up to 11.27% for Dataset 1 and nearly 21% for Dataset 2, as seen in row 2.

E_4, E_5, and E_6 evidence the small magnitudes of the signals arising in the eddy current problem as previously stated. The absolute deviations of the V_i correlation are overall less than 1.1771E-4 for Dataset 1 and below 1.5853E-4 for Dataset 2. The root mean square error E_6 penalises large errors and reduces the impact of small ones, while E_5 is more appropriate for small errors. Consequently, the absolute deviations in the predictions using the J_i and S_i correlations are below 4.0431E-1 A.m^{-2} and 2.5331E-4, respectively, among all datasets.

6.2 Application of MIT sensor design model

The proposed correlations are employed to predict the geometric combination that ensures large and stable signals from highly sensitive systems. For instance, the developed models can be used to decide between two alternative coil designs as detailed in the following case study aiming to tune the diameter of a circular coil.

Table 6. Accuracy of prediction of performance models

	V_i^{c}	$J_{i_{\sigma=1}}^{\text{c}}$	$J_{i_{\sigma=5}}^{\text{c}}$	S_i^{c}	V_i^{d}	$J_{i_{\sigma=1}}^{\text{d}}$	$J_{i_{\sigma=3}}^{\text{d}}$	$J_{i_{\sigma=5}}^{\text{d}}$	S_i^{d}
E_1[a]	0.3455	9.7781	11.1633	0.2879	0.0538	-14.6176	-17.5665	11.3386	0.7569
E_2[a]	5.4276	9.9703	11.2709	5.9772	6.6253	20.7793	17.6337	11.6268	7.9100
E_3[a]	7.1260	11.5848	12.8095	7.7600	9.5109	23.0032	18.5606	13.7733	11.5742
E_4[b]	-1.8194E-6	1.0567E-2	6.0245E-2	-1.2819E-6	1.2375E-5	-1.1866E-2	-3.8499E-2	4.0431E-1	-3.2217E-5
E_5[b]	7.7424E-5	1.1113E-2	6.1959E-2	9.7102E-5	9.6445E-5	1.6517E-2	3.8558E-2	4.0431E-1	2.5331E-4
E_6[b]	1.1771E-4	1.8048E-2	9.7946E-2	2.3962E-4	1.5853E-4	2.1579E-2	4.6450E-2	4.7432E-1	5.7766E-4
s^2	0.5066	0.3752	0.3806	0.6014	0.99045	3.1309	0.3244	0.5970	1.3338
F_{rf}	0.017	1.132	1.373	0.089	0.228	2.832	2.515	1.467	0.482

[a]Figures shown in percentages.
[b]Units: V_i is a ratio, J_i in A.m^{-2} and S_i is dimensionless.
[c]Reference values from Dataset 1.
[d]Reference values from Dataset 2.

Consider an MIT system targeting measurements of a medium of a conductivity ranging between 1 Sm^{-1} and 5 Sm^{-1}. The perimeter of the imaging region restricts the coil size to less than 45 mm. The maximum number of turns is 6 from a 0.5 mm copper wire. The application of the developed models is as follows.

a) Substitute in equation (7) the parameters of the Vi model from Table 5.
b) Specify the desired diameter $Dc = 45$ or $Dc = 35$, the number of turns $N = 6$, and the coil profile index $G = 1$ corresponding to circular helix coils. This yields

$V_{45} = (A_1(45) + A_3(6)^2 + A_5(6)^{0.5} + A_8(1) + A_9)^2 = 2.007E - 3$
$V_{35} = (A_1(35) + A_3(6)^2 + A_5(6)^{0.5} + A_8(1) + A_9)^2 = 1.130E - 3$

where subscripts '45' and '35' refer to the coil sizes under evaluation.

c) Similarly to (a) and (b), substitute the parameters a_1 to a_9 of the Ji model (see Table 5) and the coil geometric characteristics in equation (8) to calculate the maximum induction currents model:

$J_{45_{\sigma=5}} = 6.518E - 1$ A.m^{-2}
$J_{35_{\sigma=5}} = 6.254E - 1$ A.m^{-2}

d) Likewise, include the geometric parameters of interest in equation (9) to calculate the system sensitivity:

$S_{45} = 7.883E - 4$
$S_{35} = 3.229E - 4$

Based on the obtained results, the performance parameters calculated for the 45 mm sensor, are consistently superior to those of the 35 mm sensor. In particular, the voltage ratio and sensitivity factor were 1.8 and 2.4 times higher than those of the 35mm sensor, respectively.

Now for the same range of performance factors computed above, let us navigate other wire gauges and coil profile possibilities. This is achieved by simultaneously optimising the performance models via a multi-objective problem formulation given in section 2.4. There are many optimisation algorithms available. In this work two types of methods were selected to illustrate the approach: the Interior-Point Optimization (*fmincon*), and Multi-Objective Genetic Algorithm (MOGA) (*gamultiobj*) from the MATLAB™ optimisation toolbox. The procedure is the following.

a) Define the ranges of the inequality constraints as:
$Dc = [45,35]$; $dw = [0.40,0.85]$; $N = [2,6]$; $G = [1,2]$
b) Define the MIT sensors criteria by the correlations (7), (8) and (9), that is:

$$Vi = (a_1 Dc + a_3 N^2 + a_5 N^{0.5} + a_8 G + a_9)^2$$
$$Ji = 10^{(a_1 Dc + a_2 Dc^{0.5} + a_3 N^2 + a_4 N + a_5 N^{0.5} + a_7 dw^{0.5} + a_8 G + a_9)}$$
$$Si = 10^{(a_1 Dc + a_2 Dc^{0.5} + a_3 N^2 + a_4 N + a_5 N^{0.5} + a_6 dw + a_8 G + a_9)}$$

c) Deduce the objective function for the purpose of minimisation $f(x) = [-V_i(x), -J_i(x), -S_i(x)]$
d) Using *fmincon* find one solution that minimises the weighted sum of the individual objectives defined in (c):

$$f(x) = \alpha \frac{-V_i(x)}{NV} + \beta \frac{-J_i(x)}{NJ}, + \gamma \frac{-S_i(x)}{NS}$$

where the normalisation factors are NV, NJ and NS, and the weighting factors used to emphasise the relative importance of the objectives are α, β and γ, where $\alpha + \beta + \gamma = 1$

The returned results are:
$Dc = 45$ mm, $dw = 0.60$ mm, $N = 6$, and $G = 2$.

The coil diameter is in agreement with the previous calculations. The multiobjective evaluation, allows to separately evaluate each objective function and study their

relationship. Figure 6 shows the Pareto set found using the *gamultiobj* MATLAB^{TM} function. It represents a set of optimal solutions found for one run of the simulation algorithm. It illustrates the relationship between the performance correlations. The highlighted data points correspond to the solution the objective function values corresponding to the solution obtained with *fmincon* where: $Dc = 45$ mm, $dw = 0.60$ mm, $N = 6$, and $G = 2$.

7. Discussion

The correlations developed (7) – (9) contain a combination of independent variables that accounted for over 98% of the variance observed in all performance factors and showed good agreement with reference values and experimental data.
The induced voltage ratio, closely related to the signal-to-noise ratio, was found to be primarily influenced by the coil size and shape. The developed model resulted in predictions with a mean absolute error below 4% and a proximity to reference values within a 10% margin. The sensitivity of the system to changes in conductivity was strongly influenced by the number of turns and the coil size. The associated correlation demonstrated a small negative relationship between the sensitivity model prediction and the wire diameter.

The induced eddy currents had a close negative interaction to the number of turns as by Spearman coefficient and multiple regression analyses. The J_i correlation presented the poorest performance with a large mean percent error and among the highest variance figures recorded, i.e. 21% and 3% for the scenario with the lowest conductivity (1 S.m^{-1}), respectively. Overall, the error of the predictions is greater for reference values outside the initial database spectrum, hence care is advised if intended to be implemented using parameters outside the spectrum within which they were derived and as well as for heterogeneous conductivity distributions.

8. Final remarks and further work

Knowledge of the effects of varying the geometry of the coils is beneficial to enhance the design of the sensors since comprehensive studies of their effect on MIT system performance is not available in the literature. This paper derived performance models based on 90 sensor geometry combinations. The data was processed through both bivariate correlation and multiple regression analyses. The correlation factor among four geometric parameters (coil size, wide diameters, coil profile and number of turns) and three
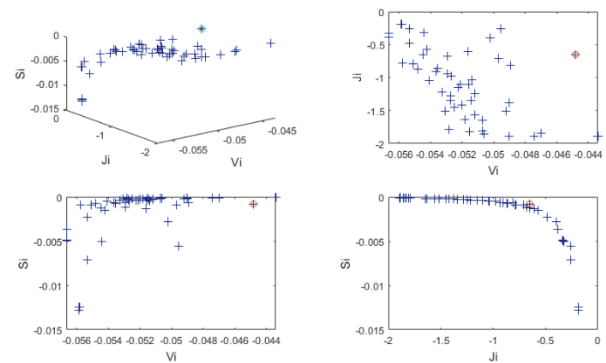
Figure 6. Illustration of the relationship between different objective functions

performance factors (voltage ratio, induced eddy currents, and sensibility) is given. The developed models resulted in predictions of the performance parameters within a ±15% deviation margin.

The case study illustrated how the application of the models could be extended to predict the level of the signal to be measured from a particular sensor design and hence provide useful information to researchers.

The incorporation of the developed correlations into optimisation algorithms with different weights for each derived model will be considered in future work. This approach will require the use of global optimisation algorithms, increasing the overall computational complexity yet allowing the automation of the sensor design process.

References

[1] L. Ma and M. Soleimani, "Magnetic induction tomography methods and aplications: a review," *Meas. Sci. Technol*, vol. 28, 2017.

[2] S. Watson, R. J. Williams, W. Gough, and H. Griffiths, "A magnetic induction tomography system for samples with conductivities below 10 S/m," *Meas. Sci. Technol.*, vol. 19, no. 1, pp. 1–11, 2008.

[3] H. Scharfetter, S. Issa, and D. Gürsoy, "Tracking of object movements for artefact suppression in Magnetic Induction Tomography (MIT)," *J. Phys. Conf. Ser.*, vol. 224, no. 1, pp. 1–5, 2010.

[4] L. Ma, D. Mccann, and A. Hunt, "Combining Magnetic Induction Tomography and Electromagnetic Velocity Tomography for Water Continuous Multiphase Flows," *IEEE Sens. J.*, vol. 17, no. 24, pp. 8271–8281, 2017.

[5] Z. Xiao, C. Tan, and F. Dong, "Effect of inter-tissue inductive coupling on multi-frequency imaging of intracranial hemorrhage by magnetic induction tomography," *Meas. Sci. Technol*, vol. 28, pp. 1–11, 2017.

[6] L. Ma, A. Hunt, and M. Soleimani, "Experimental evaluation of conductive flow imaging using magnetic induction tomography," *Int. J. Multiph. Flow*, vol. 72, pp. 198–209, 2015.

[7] M. Zolgharni, P. D. Ledger, and H. Griffiths, "Forward modelling of magnetic induction tomography: a sensitivity

study for detecting haemorrhagic cerebral stroke," *Med. Biol. Eng. Comput.*, vol. 47, no. 12, pp. 1301–1313, 2009.

[8] A. Korjenevsky, V. Cherepenin, and S. Sapetsky, "Magnetic induction tomography: experimental realization," *Physiol. Meas.*, vol. 21, no. 1, pp. 89–94, 2000.

[9] H. Scharfetter, A. Köstinger, and S. Issa, "Spectroscopic 16 channel magnetic induction tomograph : The new Graz MIT system," in *IFMBE Proceedings, vol 17.*, 2007, pp. 452–455.

[10] H. C. Wee, S. Watson, R. Patz, H. Griffiths, and R. J. Williams, "A magnetic induction tomography system with sub-millidegree phase noise and high long-term phase stability," *IFMBE Proc.*, vol. 22, pp. 744–747, 2008.

[11] M. Hamsch, C. H. Igney, and M. Vauhkonen, "16 Channel Magnetic Induction Tomography System Featuring Parallel Readout," in *IFMBE Proceedings, vol 17.*, 2007, pp. 484–487.

[12] M. Vauhkonen, M. Hamsch, and C. H. Igney, "A measurement system and image reconstruction in magnetic induction tomography," *Physiol. Meas.*, vol. 29, no. July, pp. S445–S454, 2008.

[13] H. Y. Wei and A. J. Wilkinson, "Design of a sensor coil and measurement electronics for magnetic induction tomography," *IEEE Trans. Instrum. Meas.*, vol. 60, no. 12, pp. 3853–3859, 2011.

[14] S. Lyons, K. Wei, and M. Soleimani, "Wideband precision phase detection for magnetic induction spectroscopy," *Measurement*, vol. 115, no. June 2017, pp. 45–51, 2018.

[15] D. Goss, R. O. Mackin, E. Crescenco, H. S. Tapp, and A. J. Peyton, "Understanding the coupling mechanisms in high frequency EMT," *3rd World Congr. Ind. Process Tomogr.*, pp. 364–369, 2003.

[16] Z. Zhang, H. Lei, P. Liu, and D. Zhou, "Sensitivity Study for Improved Magnetic Induction Tomography (MIT) Coil System," *Minist. Educ. People's Repub. China.*, vol. 1, no. 1, pp. 1317–1320, 2013.

[17] D. Goss, R. O. Mackin, E. Crescenco, H. S. Tapp, and A. J. Peyton, "Development of electromagnetic induction tomography (EMT) hardware for determining human body composition," *Proc. World Congr. Ind. Process Tomogr.*, pp. 377–383, 2003.

[18] Y. Arellano, L. Ma, A. Hunt, and O. Haas, "Characterisation of the Effects of Sensor Geometry on the Performance of Magnetic Induction Tomography Systems," in *9th World Congress on Industrial Process Tomography*, 2018, pp. 373–381.

[19] F. W. Grover, *Inductance calculations: working formulas and tables*. New York: D. Van Nostrand Co., 1973.

[20] M. Panik, *Statistica inference: A short course*. John Wiley & Sons, Inc, 2012.

[21] G. Corder and D. Foreman, *Nonparametric Statistics for Non-Statisticians*. New Jersey: John Wiley & Sons, Inc, 2009.

[22] M. Qualls, D. J. Pallin, and J. D. Schuur, "Parametric Versus Nonparametric Statistical Tests : The Length of Stay Example," *Acad. Emerg. Med.*, vol. 17, pp. 1113–1121, 2010.

[23] R. Ruiz, A. Brito, and J. Marquez, "Evaluation of Multiphase Flow Models To Predict Pressure Gradient in Vertical Pipes With Highly Viscous Liquids," in *Society of Petroleum Engineers*, 2014, pp. 1–8.

[24] G. Corliss, C. Faure, A. Griewank, L. Hascoet, and U. Naumann, Eds., *Automatic Differentiation of Algoritms: From simulation to optimization*. Springer, 2002.

[25] A. Bossavit, *Computational Electromagnetism: Variational Formulations, Complementarity, Edge Elements*. Academic Press, 1997.

[26] A. M. Ansari, N. D. Sylvester, C. Sarica, O. Shonham, and J. P. Brill, "A Comprehensive Mechanistic Model for Upward Two-Phase Flow in Wellbores," *SPE Prod. Facil.*, no. May, pp. 143–152, 1990.

[27] F. Garcia, R. Garcia, J. C. Padrino, C. Mata, J. L. Trallero, and D. D. Joseph, "Power law and composite power law friction factor correlations for laminar and turbulent gas-liquid flow in horizontal pipelines," *Int. J. Multiph. Flow*, vol. 29, no. 2, pp. 1605–1624, 2003.